International Journal of Control
Vol. 00, No. 00, DD Month 200x, 1–20

Control of coordinated patterns for ocean sampling

FUMIN ZHANG†, DAVID M. FRATANTONI‡, DEREK A. PALEY†, JOHN M. LUND‡, NAOMI EHRICH LEONARD*†
†Department of Mechanical and Aerospace Engineering
Princeton University
Princeton, NJ 08544, USA
{fzhang, dpaley, naomi}@princeton.edu
‡ Department of Physical Oceanography
Woods Hole Oceanographic Institution
Woods Hole, MA 02543, USA
{dfratantoni, jlund}@whoi.edu
(*Received 00 Month 200x; In final form 00 Month 200x*)

A class of underwater vehicles are modelled as Newtonian particles for navigation and control. We show a general method that controls cooperative Newtonian particles to generate patterns on closed smooth curves. These patterns are chosen for good sampling performance using mobile sensor networks. We measure the spacing between neighbouring particles by the relative curve phase along the curve. The distance between a particle and the desired curve is measured using an orbit function. The orbit value and the relative curve phase are then used as feedback to control motion of each particle. From an arbitrary initial configuration, the particles converge asymptotically to form an invariant pattern on the desired curves. We describe application of this method to control underwater gliders in a field experiment in Buzzards Bay, MA in March 2006.

1 Introduction

Technological advances make it possible today to use fleets of sensor-equipped autonomous underwater vehicles (AUVs) to collect oceanographic data in efficient and intelligent ways never before available. For example, throughout August 2003, as part of the Autonomous Ocean Sampling Network (AOSN) field experiment, as many as twelve underwater gliders were used simultaneously to collect data near Monterey Bay, California. This data was assimilated into ocean models that computed real-time predictions of the coupled physical and biological dynamics in the Monterey Bay region. The data set produced in August 2003 is uniquely rich and revealing, c.f. MBARI (2003).

Adaptive sampling refers to the ability to modify the design of sampling networks during the course of operation in response to measurements and real-time model estimation and predictions. Critical to successful adaptive sampling is the coordination of the multiple vehicles (mobile sensors) that make up the network. For instance, if the vehicles get too close to one another they take redundant measurements. In order to get the greatest advantage from the fleet, the vehicles should share information on their whereabouts and their observations and cooperate to best meet sampling objectives. More details can be found in a recent paper Leonard et al. (2005) and the references therein. In August 2006 in Monterey Bay, ten gliders were coordinated to move on patterns that adapted in response to changes in the ocean. This field experiment was part of the Adaptive Sampling and Prediction (ASAP) project c.f. Princeton (2003).

In this paper, based on our previous work in Zhang and Leonard (2006), we present both analytical and experimental results on achieving desired patterns on closed curves using a Newtonian particle model for idealised vehicles. The Newtonian particle model is adopted because vehicle trajectories are usually measured in kilometres, whereas the vehicle dimensions are typically measured in metres. We rigorously define invariant patterns on closed curves that are smooth and topologically simple, i.e. on curves that have only one loop and no self intersections. In an invariant pattern, all particles are on curves of certain class, and the relative curve length between each pair of particles is constant over time. We design a feedback

control law to achieve such an invariant pattern from an arbitrary initial configuration of the particles. The control law can either be directly applied to control ocean vehicles or be used to plan paths and waypoints to guide those vehicles. In the latter case the autopilot on board the vehicle is responsible for producing appropriate control commands to follow the prescribed waypoints.

Underwater gliders are a class of autonomous underwater vehicles (AUVs) that are propelled by changing buoyancy and pitch in a periodic manner. We have developed methods for applying the control design to plan paths and waypoints for coordinating the motion of underwater gliders. Our methods have been tested on two gliders in a recent experiment in Buzzards Bay, MA.

Our methods to generate coordinated patterns may also be used for applications such as the detection and surveillance of natural boundaries using multiple sensor platforms. Other recent developments for this purpose can be found in Bertozzi et al. (2005), Hsieh and Kumar (2005), Zarzhitsky et al. (2005), Andersson and Park (2005), Clark and Fierro (2006) and Susca et al. (2006). In those papers coherent patterns are established using methods that are different from ours. Results in this paper provide a general theoretical framework in developing means for systematic pattern generation on closed curves.

In Section 2, we show that the particle model can be rewritten as a system under speed and steering control. In Section 3, the relative motion between a controlled particle and a family of closed curves is studied. We derive a control law based on a Lyapunov function to achieve invariant patterns for N particles in Section 4, and prove the convergence of the controlled dynamics to the desired pattern. In Section 5, simulation results are obtained for adaptive sampling experiments in Monterey Bay. We present results from the Buzzards Bay experiment in section 6.

2 Particle Model

Consider the motion of the centre of mass (COM) of a vehicle moving in the plane. We view each vehicle as a Newtonian particle with unit mass that obeys $\ddot{\boldsymbol{r}} = \boldsymbol{f}$ where $\boldsymbol{r} \in \mathbb{R}^2$ and $\boldsymbol{f}$ is the total external force. The state of a particle is $(\boldsymbol{r}, \dot{\boldsymbol{r}})$. If $\dot{\boldsymbol{r}}$ does not vanish, then we can define a unit vector $\boldsymbol{x} = \dot{\boldsymbol{r}} / \parallel \dot{\boldsymbol{r}} \parallel$. We also define

$$\boldsymbol{y} = \begin{bmatrix} 0 & -1 \\ 1 & 0 \end{bmatrix} \boldsymbol{x} \ . \tag{1}$$

Such $\boldsymbol{y}$ is a unit vector perpendicular to $\boldsymbol{x}$. Therefore $\boldsymbol{f}$ can be expressed as

$$\boldsymbol{f} = \alpha^2 u \boldsymbol{y} + v \boldsymbol{x} \tag{2}$$

where we define $\alpha = \parallel \dot{\boldsymbol{r}} \parallel$, $\alpha^2 u = \boldsymbol{f} \cdot \boldsymbol{y}$ and $v = \boldsymbol{f} \cdot \boldsymbol{x}$. On the other hand, we compute

$$\ddot{\boldsymbol{r}} = \frac{\mathrm{d}}{\mathrm{d}t}(\alpha \boldsymbol{x}) = \dot{\alpha} \boldsymbol{x} + \alpha \dot{\boldsymbol{x}} \tag{3}$$

which implies that

$$\begin{aligned} \dot{\alpha} + \alpha \dot{\boldsymbol{x}} \cdot \boldsymbol{x} &= \boldsymbol{f} \cdot \boldsymbol{x} = v \\ \alpha \dot{\boldsymbol{x}} \cdot \boldsymbol{y} &= \boldsymbol{f} \cdot \boldsymbol{y} = \alpha^2 u \ . \end{aligned} \tag{4}$$

Since $\boldsymbol{x}$ is a unit vector, we have $\dot{\alpha} = \boldsymbol{f} \cdot \boldsymbol{x} = v$, and the time derivative of $\boldsymbol{x}$ can be computed as follows:

$$\dot{\boldsymbol{x}} = \frac{\mathrm{d}}{\mathrm{d}t} \frac{\dot{\boldsymbol{r}}}{\parallel \dot{\boldsymbol{r}} \parallel} = \frac{\boldsymbol{f}}{\alpha} - \frac{\boldsymbol{f} \cdot \boldsymbol{x}}{\alpha} \boldsymbol{x} = \alpha u \boldsymbol{y} \ . \tag{5}$$

The time derivative of $\boldsymbol{y}$ is

$$\dot{\boldsymbol{y}} = \begin{bmatrix} 0 & -1 \\ 1 & 0 \end{bmatrix} (\alpha u \boldsymbol{y}) = -\alpha u \boldsymbol{x} \ . \tag{6}$$

We conclude that if the speed α of a Newtonian particle is non-zero, then the motion of the particle can be described as

$$\begin{aligned} \dot{\boldsymbol{r}} &= \alpha \boldsymbol{x} \\ \dot{\boldsymbol{x}} &= \alpha u \boldsymbol{y} \\ \dot{\boldsymbol{y}} &= -\alpha u \boldsymbol{x} \\ \dot{\alpha} &= v \ . \end{aligned} \tag{7}$$

The advantage of using these equations instead of $\ddot{\boldsymbol{r}} = \boldsymbol{f}$ comes from the fact that u can be viewed as the steering control and v can be viewed as the speed control, and the steering dynamics are separated from the speed dynamics.

We note that even if we let $\alpha = 0$ in equations (7), the system appears to agree with Newton's equation $\ddot{\boldsymbol{r}} = \boldsymbol{f}$ if $\boldsymbol{f}$ does not vanish i.e. $v \neq 0$. In this case we choose $\boldsymbol{x} = \boldsymbol{f} / \| \boldsymbol{f} \|$. However, in this case, there may exist discontinuities in the orientation of the frame formed by $\boldsymbol{x}$ and $\boldsymbol{y}$.

3 Particle and Closed Curves

Suppose we are given a family of closed regular curves $\mathcal{C}(\sigma, z)$ with σ and z functions in the plane satisfying the following conditions:

(AS1) There exists a bounded open set B such that all curves in $\mathcal{C}$ belong to B and any point in B belongs to a unique curve in $\mathcal{C}$.

(AS2) On the set B, z is a C^2 smooth function. The value of z is bounded below by a real number $z_{\min}$ and bounded above by $z_{\max} > z_{\min}$ i.e. $z \in (z_{\min}, z_{\max})$. The closed curves in $\mathcal{C}$ are the level curves of function z. We further assume that $\| \nabla z \| \neq 0$ on the set B. We call z the *orbit function*.

(AS3) There exists a regular curve Γ that intersects each curve in $\mathcal{C}$ at a unique point. We call these intersections the *starting points*.

(AS4) σ is the *curve length parameter* for a unique curve in $\mathcal{C}$ measured from the starting point.

One example of such a family is the family of ellipses given by $r_x^2 + e\, r_y^2 = z$ where $e > 0$ is the eccentricity of the ellipses (see Figure 1). If we select $z_{\min} > 0$ and $z_{\max}$ to be a finite number greater than $z_{\min}$ then this family satisfies the conditions (AS1) and (AS2) with

$$B = \{(r_x, r_y) \in \mathbb{R}^2 | z_{\min} < r_x^2 + e\, r_y^2 < z_{\max}\}. \tag{8}$$

The positive horizontal axis can be viewed as Γ and σ can be chosen as the curve length parameter of any ellipse in the family. Hence (AS3) and (AS4) are also satisfied.

Along the trajectory of a moving particle in the set B, the value of z is changing with respect to time. We have

$$\dot{z} = \nabla z \cdot \dot{\boldsymbol{r}} = -\alpha \| \nabla z \| \sin \phi \tag{9}$$

where we define

$$\sin \phi = -\frac{\nabla z}{\| \nabla z \|} \cdot \boldsymbol{x} \ . \tag{10}$$

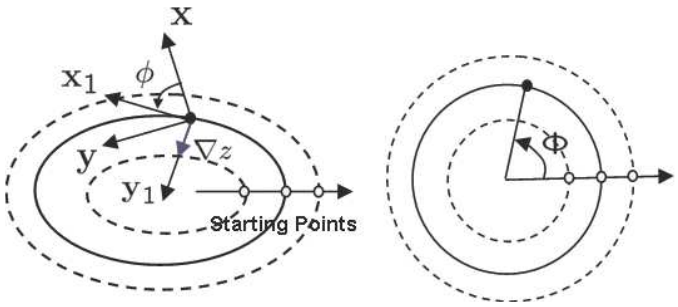

Figure 1. *The relative motion between a particle and a family of ellipses; each ellipse is a level curve of some function z. The solid dot represents the particle and the hollow dots represent the starting points. The frames* $(\boldsymbol{x}, \boldsymbol{y})$ *and* $(\boldsymbol{x}_1, \boldsymbol{y}_1)$ *are illustrated and the angle* ϕ *measures the difference in their orientation. The arc-length* s *is the length of the curve segment between the starting point and the particle. If we map the ellipses to circles preserving arc-length (picture on right), then* Φ *can be visualised as the phase angle on the circles.*

The angle ϕ is the angle between the velocity vector of the particle and the tangent vector to the curve determined by z. For convenience we let $\boldsymbol{x}_1$ denote this tangent vector and $\boldsymbol{y}_1 = \nabla z / \| \nabla z \|$. The direction of $\boldsymbol{x}_1$ is selected so that $\boldsymbol{x}_1$ and $\boldsymbol{y}_1$ form a right handed coordinate system with $\boldsymbol{x}_1 \times \boldsymbol{y}_1$ pointing to the reader as shown in Figure 1. Then along the trajectory of the moving particle, the vector $\boldsymbol{y}_1$ changes as

$$\begin{aligned} \dot{\boldsymbol{y}}_1 &= \left(\frac{\nabla^2 z\, \dot{\boldsymbol{r}}}{\| \nabla z \|} - \frac{(\nabla z \cdot \nabla^2 z\, \dot{\boldsymbol{r}}) \nabla z}{\| \nabla z \|^3} \right) \\ &= \frac{\alpha}{\| \nabla z \|} \left(\nabla^2 z \boldsymbol{x} - (\boldsymbol{y}_1 \cdot \nabla^2 z\, \boldsymbol{x}) \boldsymbol{y}_1 \right) \end{aligned} \tag{11}$$

where $\nabla^2 z$ is the Hessian matrix of function $z(\boldsymbol{r})$. Taking the time derivative of $\sin\phi = \boldsymbol{y}_1 \cdot \boldsymbol{x}$ yields

$$\begin{aligned} \cos\phi\, \dot{\phi} &= -\dot{\boldsymbol{x}} \cdot \boldsymbol{y}_1 - \boldsymbol{x} \cdot \dot{\boldsymbol{y}}_1 \\ &= -(\alpha u \boldsymbol{y}) \cdot \boldsymbol{y}_1 - \boldsymbol{x} \cdot \dot{\boldsymbol{y}}_1 \\ &= -\alpha u \cos\phi - \\ &\quad \frac{\alpha}{\| \nabla z \|} \left(\boldsymbol{x} \cdot \nabla^2 z \boldsymbol{x} + (\boldsymbol{y}_1 \cdot \nabla^2 z\, \boldsymbol{x}) \sin\phi \right). \end{aligned} \tag{12}$$

Considering that $\boldsymbol{x} = \cos\phi\, \boldsymbol{x}_1 - \sin\phi \boldsymbol{y}_1$, we know that

$$\begin{aligned} &\boldsymbol{x} \cdot \nabla^2 z \boldsymbol{x} + (\boldsymbol{y}_1 \cdot \nabla^2 z\, \boldsymbol{x}) \sin\phi \\ &= \cos^2\phi (\boldsymbol{x}_1 \cdot \nabla^2 z \boldsymbol{x}_1) - \sin\phi \cos\phi (\boldsymbol{x}_1 \cdot \nabla^2 z\, \boldsymbol{y}_1). \end{aligned} \tag{13}$$

Therefore,

$$\dot{\phi} = \alpha \left(\kappa_1 \cos\phi + \kappa_2 \sin\phi - u \right) \tag{14}$$

where we define

$$\begin{aligned} \kappa_1 &= -\frac{1}{\| \nabla z \|} \boldsymbol{x}_1 \cdot \nabla^2 z\, \boldsymbol{x}_1 \\ \kappa_2 &= \frac{1}{\| \nabla z \|} \boldsymbol{x}_1 \cdot \nabla^2 z\, \boldsymbol{y}_1 \,. \end{aligned} \tag{15}$$

We let s be the curve length of a curve in the family measured from the starting point. The curve length s is a function of σ and z. Since all curves in $\mathcal{C}$ are closed, the total curve length L of each curve is finite and a function of z. As the particle moves, the variation of the curve length is

$$\dot{s} = \frac{\partial s}{\partial \sigma} \dot{\sigma} + \frac{\partial s}{\partial z} \dot{z}$$

$$
\begin{aligned}
&= \left.\frac{\mathrm{d}s}{\mathrm{d}t}\right|_{z=\text{const}} + \frac{\partial s}{\partial z}\dot{z} \\
&= \alpha\cos\phi - \alpha\frac{\partial s}{\partial z}\parallel\nabla z\parallel\sin\phi\,. \qquad (16)
\end{aligned}
$$

The total curve length L is a function of z only. Its variation is

$$
\dot{L} = \frac{\partial L}{\partial z}\dot{z} = -\alpha\frac{\partial L}{\partial z}\parallel\nabla z\parallel\sin\phi\,. \qquad (17)
$$

Analogous to the concept of mean anomaly used for satellite formation control in Zhang and Krishnaprasad (2004), we define the curve phase variable

$$
\Phi = 2\pi\frac{s}{L}\,, \qquad (18)
$$

which was also used in Zhang and Leonard (2006) and Paley et al. (2006a). This angle, with its value belongs to the interval $[0, 2\pi)$, is measured from the starting point of each curve, and it can be visualised as shown in Figure 1. The time derivative of Φ is

$$
\begin{aligned}
\dot{\Phi} &= 2\pi\left(\frac{\dot{s}}{L} - \frac{s}{L^2}\dot{L}\right) \\
&= \frac{2\pi\,\alpha}{L}\cos\phi - \frac{2\pi\,\alpha}{L}\left(\frac{\partial s}{\partial z} - \frac{s}{L}\frac{\partial L}{\partial z}\right)\dot{z}. \qquad (19)
\end{aligned}
$$

On the other hand, the time derivative of Φ can also be computed as

$$
\dot{\Phi} = \left.\frac{\mathrm{d}\Phi}{\mathrm{d}t}\right|_{z=\text{const}} + \frac{\partial\Phi}{\partial z}\dot{z}. \qquad (20)
$$

Comparing (19) and (20), we can observe that

$$
\frac{\partial\Phi}{\partial z} = \frac{2\pi\,\alpha}{L}P \qquad (21)
$$

where we define

$$
P = -\left(\frac{\partial s}{\partial z} - \frac{s}{L}\frac{\partial L}{\partial z}\right). \qquad (22)
$$

Using z, ϕ, Φ and α to describe the state of the particle, we summarise the system equations for one particle as follows:

$$
\begin{aligned}
\dot{z} &= -\alpha\parallel\nabla z\parallel\sin\phi \\
\dot{\phi} &= \alpha(\kappa_1\cos\phi + \kappa_2\sin\phi - u) \\
\dot{\Phi} &= \frac{2\pi\,\alpha}{L}\left(\cos\phi + P\parallel\nabla z\parallel\sin\phi\right) \\
\dot{\alpha} &= v. \qquad (23)
\end{aligned}
$$

4 Achieving Patterns

Now consider the motion of N particles in the bounded open set B. For $i = 1, ..., N$, the ith particle satisfies equation (23) indexed by i. We define an invariant pattern for these particles.

Definition 4.1 We say N particles form an *invariant pattern* determined by $(\boldsymbol{c}_z, \boldsymbol{c}_s, c_v)$ if $(z_i, \phi_i, \Phi_i, \alpha_i)$ satisfies

$$\begin{aligned} & z_i = c_{zi} \\ & \phi_i = 0 \\ & \Phi_j - \Phi_{j+1} = c_{sj} \\ & \min_i\{\alpha_i\} = c_v \end{aligned} \tag{24}$$

for all $i = 1, ..., N$ and $j = 1, ..., N-1$. Here c_{zi} is the ith component for the N dimensional constant vector $\boldsymbol{c}_z$, and c_{sj} is the jth component for the $N-1$ dimensional constant vector $\boldsymbol{c}_s$. The constants satisfy $c_v > 0$, $z_{\min} < c_{zi} < z_{\max}$ and $0 < c_{sj} < 2\pi$.

We design control laws for (u_i, v_i) so that from an arbitrary initial configuration, the particles achieve a given pattern asymptotically. Our control laws are based on control Lyapunov functions.

Let $h_{zi}(z)$ be a smooth function on $(z_{\min}, z_{\max})$ and $f_{zi}(z) = \frac{d\,h_{zi}}{dz}$ satisfying the following conditions:

(AS5) $\lim_{z\to z_{\min}} h_{zi}(z) = \lim_{z\to z_{\max}} h_{zi}(z) = +\infty$.
(AS6) $f_{zi}(z)$ is a monotone increasing smooth function with $f_{zi}(z) = 0$ if and only if $z = c_{zi}$.

Function $f_{zi}(z)$ can be constructed as

$$\begin{aligned} f_{zi}(z) = \tan\left(\frac{\pi(2z - z_{\max} - z_{\min})}{2(z_{\max} - z_{\min})}\right) - \\ \tan\left(\frac{\pi(2c_{zi} - z_{\max} - z_{\min})}{2(z_{\max} - z_{\min})}\right). \end{aligned} \tag{25}$$

We let $h_{sj}(\Phi)$ be a smooth function on $(0, 2\pi)$ and $f_{sj}(\Phi) = \frac{d\,h_{sj}}{d\Phi}$ satisfying the following conditions:

(AS7) $\lim_{\Phi\to 0} h_{sj}(\Phi) = \lim_{\Phi\to 2\pi} h_{sj}(\Phi) = +\infty$
(AS8) $f_{sj}(\Phi)$ is a monotone increasing smooth function with $f_{sj}(\Phi) = 0$ if and only if $\Phi = c_{sj}$.

We let $h_a(\alpha)$ be a smooth function on $(0, +\infty)$ and $f_a(\alpha) = \frac{d\,h_a}{d\alpha}$ satisfying the following conditions:

(AS9) $\lim_{\alpha\to 0} h_a(\alpha) = \lim_{\alpha\to+\infty} h_a(\alpha) = +\infty$
(AS10) $f_a(\alpha)$ is a monotone increasing smooth function with $f_a(\alpha) = 0$ if and only if $\alpha = c_v$.

Without loss of generality, we assume that the curve corresponding to $z_1 = c_{z1}$ has the minimum length among the curves determined by $\boldsymbol{c}_z$. Intuitively, in order to maintain the invariant pattern, the particle indexed by 1 on this shortest curve has to travel at the minimum speed among all particles. We will justify this intuition later.

Consider the following Lyapunov candidate function:

$$\begin{aligned} V = \sum_{i=1}^{N}\left(-\log\left(\cos^2\frac{\phi_i}{2}\right) + h_{zi}(z_i)\right) + \\ \sum_{j=1}^{N-1}\left(h_{sj}\left(\Phi_j - \Phi_{j+1}\right) + \frac{1}{2}\left(\frac{\alpha_j}{L_j} - \frac{\alpha_{j+1}}{L_{j+1}}\right)^2\right) + \\ h_a(\alpha_1)\,. \end{aligned} \tag{26}$$

This function consists of several positive definite terms. The term $-\log\left(\cos^2\frac{\phi_i}{2}\right)$ contributes to aligning the velocity vector of particle i with the tangent vector of the desired path. It vanishes when $\phi_i = 0$. The term $h_{zi}(z_i)$ guides particle i to the desired curve from any initial position. It vanishes when $z_i = c_{zi}$. The term $h_{sj}\left(\Phi_j - \Phi_{j+1}\right)$ corrects curve phase difference between particles j and $j+1$. It vanishes when $\Phi_j - \Phi_{j+1} = c_{sj}$. The term $h_a(\alpha_1)$ establishes the speed for particle 1. It vanishes when $\alpha_1 = c_v$. The term

$\left(\frac{\alpha_j}{L_j} - \frac{\alpha_{j+1}}{L_{j+1}}\right)^2$ enforces the correct speed relation between particles j and $j+1$. It vanishes if $\frac{\alpha_j}{L_j} = \frac{\alpha_{j+1}}{L_{j+1}}$.

This Lyapunov function candidate is based on the Lyapunov function for boundary tracking and obstacle avoidance for a single vehicle first proposed in Zhang et al. (2004). Similar functions have also been used for formation control of unit speed particles as in Justh and Krishnaprasad (2002) and Justh and Krishnaprasad (2004). Our contribution here is to introduce the coupling terms controlling relative separation and speed between vehicles. The Lyapunov function is designed so that the invariant pattern defined by (24) is a critical point. We will show that V remains finite if V is initially finite and thus ϕ_i can never be π for all $i = 1, 2, ..., N$ and L_j can never be 0 for all $j = 1, 2, ..., N-1$. Likewise, z_i remains in $(z_{\min}, z_{\max})$, $\Phi_j - \Phi_{j+1}$ remains in $(0, 2\pi)$ and α_1 is never zero.

In Appendix A, we derive control laws based on the Lyapunov function V such that

$$\begin{aligned}\dot{V} = &\sum_{i=1}^{N}\left(-\mu_1\frac{\alpha_i \sin^2\frac{\phi_i}{2}}{\cos\frac{\phi_i}{2}}\right) - \sum_{j=1}^{N-1}\mu_2\left(\frac{\alpha_j}{L_j} - \frac{\alpha_{j+1}}{L_{j+1}}\right)^2 \\ &-\mu_3 f_a(\alpha_1)^2 \le 0,\end{aligned} \tag{27}$$

where μ_1, μ_2 and μ_3 are positive constants. The steering control laws for $i = 1, 2, ..., N$ are

$$\begin{aligned}u_i = &\kappa_{1i}\cos\phi_i + \kappa_{2i}\sin\phi_i - 2f_{zi}\parallel\nabla z_i\parallel\cos^2\frac{\phi_i}{2} - \\ &2\pi(f_{si} - f_{s(i-1)})\left(\frac{1}{L_i}\sin\phi_i + 2\frac{P_i}{L_i}\parallel\nabla z_i\parallel\cos^2\frac{\phi_i}{2}\right) \\ &+\mu_1\sin\frac{\phi_i}{2}\end{aligned} \tag{28}$$

where we use f_{zi} as abbreviated notations for $f_{zi}(z_i)$. The speed control law for particle 1 is

$$v_1 = -\mu_3 f_a(\alpha_1). \tag{29}$$

For particles $j+1$ where $j = 1, 2, ..., N-1$, we compute the speed control using the following set of equations:

$$\begin{aligned}\bar{v}_1 &= v_1 + \frac{\alpha_1^2}{L_1}\frac{\partial L_1}{\partial z_1}\parallel\nabla z_1\parallel\sin\phi_1 \\ \bar{v}_{j+1} &= \frac{L_{j+1}}{L_j}\bar{v}_j + 2\pi f_{sj}L_{j+1} + \mu_2\left(\frac{L_{j+1}}{L_j}\alpha_j - \alpha_{j+1}\right) \\ v_{j+1} &= \bar{v}_{j+1} - \frac{\alpha_{j+1}^2}{L_{j+1}}\frac{\partial L_{j+1}}{\partial z_{j+1}}\parallel\nabla z_{j+1}\parallel\sin\phi_{j+1}\end{aligned} \tag{30}$$

where we use f_{sj} as abbreviated notations for $f_{sj}(\Phi_j - \Phi_{j+1})$, and use $\bar{v}_1$ and $\bar{v}_{j+1}$ as intermediate variables.

Under the control laws (28), (29), and (30), the closed-loop systems for z_i are

$$\dot{z}_i = -\alpha_i\parallel\nabla z_i\parallel\sin\phi_i, \tag{31}$$

and the closed loop systems for ϕ_i are

$$\begin{aligned}\dot{\phi}_i = \alpha_i\Bigg(&-\mu_1\sin\frac{\phi_i}{2} + 2f_{zi}\parallel\nabla z_i\parallel\cos^2\frac{\phi_i}{2} + \\ &2\pi(f_{si} - f_{s(i-1)})\left(\frac{1}{L_i}\sin\phi_i + 2\frac{P_i}{L_i}\cos^2\frac{\phi_i}{2}\right)\Bigg)\end{aligned} \tag{32}$$

for $i = 1, 2, ..., N$. The closed loop dynamics for the relative curve phase angles are

$$\begin{aligned}&\dot{\Phi}_j - \dot{\Phi}_{j+1}\\ &= 2\pi \left(\frac{\alpha_j}{L_j} \cos\phi_j - \frac{\alpha_{j+1}}{L_{j+1}} \cos\phi_{j+1} - \right.\\ &\left. \frac{\alpha_j P_j}{L_j} \parallel \nabla z_j \parallel \sin\phi_j + \frac{\alpha_{j+1} P_{j+1}}{L_{j+1}} \parallel \nabla z_{j+1} \parallel \sin\phi_{j+1} \right)\end{aligned} \tag{33}$$

for $j = 1, 2, ..., N-1$. The speed α_1 satisfies

$$\dot{\alpha}_1 = -\mu_3 f_a(\alpha_1). \tag{34}$$

To describe the relative speed between particles, we treat $\left(\frac{\alpha_j}{L_j} - \frac{\alpha_{j+1}}{L_{j+1}}\right)$ as state variables. Their closed-loop dynamics have a simple form:

$$\frac{\mathrm{d}}{\mathrm{d}t}\left(\frac{\alpha_j}{L_j} - \frac{\alpha_{j+1}}{L_{j+1}}\right) = -\mu_2 \left(\frac{\alpha_j}{L_j} - \frac{\alpha_{j+1}}{L_{j+1}}\right) - 2\pi f_{sj} \ . \tag{35}$$

We observe that μ_1, μ_2 and μ_3 are controller gains. The gain μ_1 affects the convergence rate of the alignment angle ϕ_i. The gain μ_2 affects the convergence rate of the speed difference between the particles. The gain μ_3 affects the convergence rate of the speed of the first particle to the desired speed. In practice, these gains are adjusted according to the desired performance of the vehicles.

The following theorem shows that under the above control laws, the closed-loop dynamics converge to the invariant pattern.

THEOREM 4.2 *Consider an invariant pattern given by $(\boldsymbol{c}_z, \boldsymbol{c}_s, c_v)$ and (24). Assume that conditions (AS1)-(AS10) hold and the initial conditions of N Newtonian particles in the plane are such that the initial value of V given by (26) is finite. Suppose further that $\alpha_i(t) > 0$ for all t and $i = 2, ..., N$. Then, the invariant pattern is achieved asymptotically by the system of N particles under the control laws (28), (29), and (30).*

Proof It is easy to check that the Lyapunov function V has compact sub-level sets. Under the feedback control laws defined by (28), (29), and (30), starting in the compact sub-level set determined by the finite initial value of the function V, the closed-loop system equations (31)–(35) are Lipschitz continuous in the sub-level set and piecewise Lipschitz continuous with respect to time. Therefore a solution exists and is unique. Since the value of the Lyapunov function is time-independent and non-increasing, we conclude that if the initial value of V is finite, then the entire solution stays in the sub-level set so that V is finite for all time. This and conditions (AS7) and (AS9) imply that along such a solution, the speed of the first particle satisfies $\alpha_1 > 0$ and the phase differences satisfy $\Phi_j - \Phi_{j+1} \neq 0$ for $j = 1, 2, ..., N-1$.

Applying Theorem 8.4 on page 323 in Khalil (2001), we conclude that as $t \to \infty$, the controlled system converges to the set D where $\dot{V} = 0$. This set is equivalent to

$$\phi_i = 0, \ \alpha_1 = c_v, \quad \text{and} \ \frac{\alpha_j}{L_j} = \frac{\alpha_{j+1}}{L_{j+1}} \tag{36}$$

where $i = 1, 2, ..., N$ and $j = 1, 2, ..., N-1$. On this set D, equation (35) becomes

$$\frac{\mathrm{d}}{\mathrm{d}t}\left(\frac{\alpha_j}{L_j} - \frac{\alpha_{j+1}}{L_{j+1}}\right) = -2\pi f_{sj} \ , \tag{37}$$

and equation (32) is now

$$\dot{\phi}_i = 2\alpha_i f_{zi} \parallel \nabla z_i \parallel + 4\pi\alpha_i (f_{si} - f_{s(i-1)}) \frac{P_i}{L_i}. \tag{38}$$

In order to show that $\Phi_j - \Phi_{j+1} \to c_{sj}$ and $z_i \to c_{zi}$, we need the facts that $\dot{\phi}_i \to 0$ and

$$\frac{\mathrm{d}}{\mathrm{d}t}\left(\frac{\alpha_j}{L_j} - \frac{\alpha_{j+1}}{L_{j+1}}\right) \to 0. \tag{39}$$

We first prove that (39) holds. As $t \to \infty$, since the closed loop dynamics converge to the set D where (36) is satisfied, then (33) becomes

$$\dot{\Phi}_j - \dot{\Phi}_{j+1} = 0 \tag{40}$$

which implies that $(\Phi_j - \Phi_{j+1})$ are constant. Therefore $f_{sj}(\Phi_j - \Phi_{j+1})$ are constant functions of the time t. Thus, $\frac{\mathrm{d}}{\mathrm{d}t}\left(\frac{\alpha_j}{L_j} - \frac{\alpha_{j+1}}{L_{j+1}}\right)$ converge to constant functions of time t. These constant functions must be 0 because $\left(\frac{\alpha_j}{L_j} - \frac{\alpha_{j+1}}{L_{j+1}}\right)$ converges to 0.

Then equation (39) and (37) imply that $f_{sj} \to 0$. Thus by condition (AS8), we conclude that $\Phi_j - \Phi_{j+1} \to c_{sj}$. Next, we prove that $\dot{\phi}_i \to 0$ as $t \to +\infty$. We have proved that $f_{si} \to 0$ for all i. Then from (38) we observe, on the set D,

$$\dot{\phi}_i(t) = 2\alpha_i f_{zi} \,\|\, \nabla z_i \,\|\,. \tag{41}$$

Since z_i and α_i are constant on the set D, f_{zi} are constant for all i. Then $\| \nabla z_i \|$ is a smooth periodic function of time t as particle i moves along the orbit determined by z_i in constant speed α_i. Therefore, $\| \nabla z_i \|$ are uniformly continuous with respect to time for all i. We can apply an extension of the Barbalat lemma proved in Micaelli and Samson (1993). According to this extended Barbalat lemma, we conclude that $\dot{\phi}_i(t) \to 0$ because $\dot{\phi}_i(t)$ converges to a uniformly continuous function and $\phi_i(t) \to 0$.

The fact that $\dot{\phi}_i \to 0$ implies that $f_{zi} \to 0$ because $\alpha_i \neq 0$ and by condition (AS2), $\| \nabla z_i \| \neq 0$. By condition (AS6), we conclude that $z_i \to c_{zi}$ for $i = 1, 2, ..., N$. □

Remark 1 Notice that all our arguments are based on the assumptions that $\alpha_i(t) > 0$ for $i = 2, 3, ..., N$ (with $\alpha_1(t) > 0$ guaranteed by the finiteness of the Lyapunov function). These assumptions are not very difficult to be satisfied if the initial speed for each of the particles is large enough and the desired speed for the first particle is also large enough. We have observed convergence in simulations even if $\alpha_i = 0$ for some i at certain time instances.

Remark 2 The condition (AS7) and the finiteness of the Lyapunov function V prevent the curve phase difference $(\Phi_j - \Phi_{j+1})$ from being 0 or 2π. This implies that particle j will not collide with particle $j-1$ or particle $j+1$.

Remark 3 After linearising the closed-loop dynamics, we observe that the closed-loop system is exponentially stable within a neighbourhood of the equilibrium. An input-to-state stability result may be derived from this observation. Hence the control law is robust under bounded perturbations.

5 Simulations

Our control laws are designed to coordinate mobile sensor networks for ocean sampling. One class of closed curves that plays an important role in the ASAP field experiments is the class of super-ellipses. A super-ellipse looks like a rectangular box with rounded corners. Oceanographers who operate AUVs are interested in the super-ellipses because large segments of the curve are almost straight lines. In addition, the almost rectangular shape allows one to easily divide a large region into smaller rectangular blocks. As ocean dynamics change, an AUV can be directed from patrol of the boundary curve of a large block to patrol of a smaller block, etc.

We simulate such a scenario with our controlled particle model and plot the tracks and snapshots of the vehicles (modelled as Newtonian particles) on a map of a region near Monterey Bay, CA where the ASAP

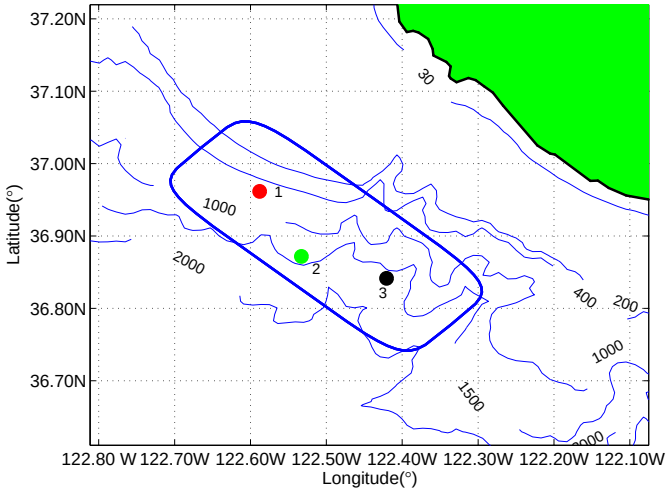

Figure 2. *The initial positions of the three vehicles and the desired super-elliptic track. The horizontal axis and the vertical axis indicate longitude and latitude, respectively.*

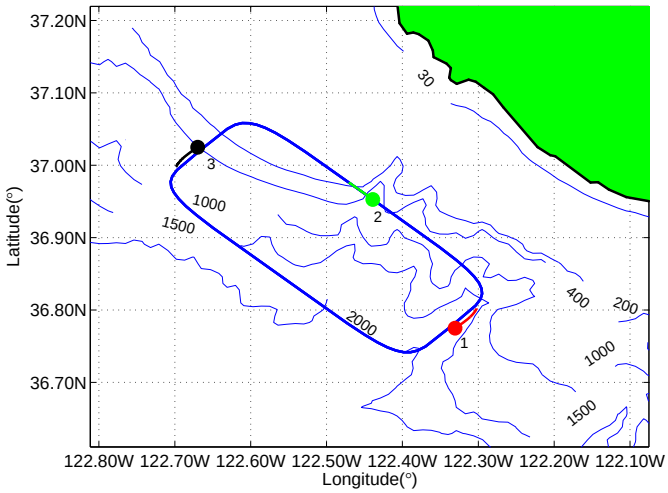

Figure 3. *The three vehicles move counter-clockwise on the desired 40km by 16km super-elliptic track.*

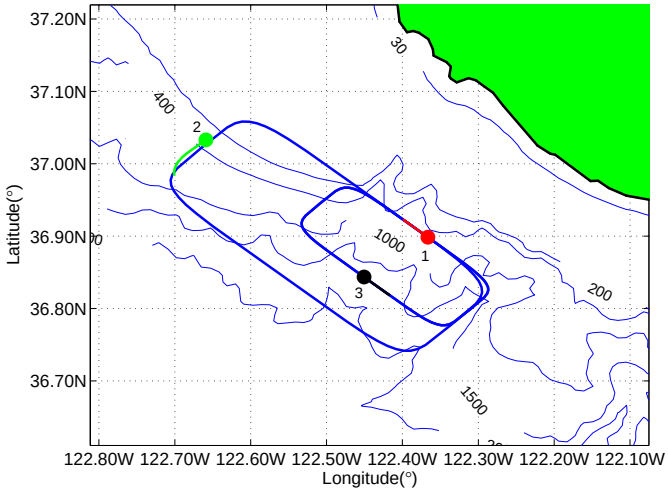

Figure 4. *Vehicles 1 and 3 move on a 12km by 4.8km super-elliptic box and vehicle 2 moves on the 40km by 16km box.*

2006 field experiments were held. In the first example, three vehicles are controlled to patrol a 40km by 16km super-elliptic box. Furthermore, vehicles 1 and 2 and vehicles 2 and 3 are to be separated along the track such that $\Phi_1 - \Phi_2 = \Phi_2 - \Phi_3 = c_{s1} = c_{s2} = \pi/2$. The minimum speed for the vehicles is $c_v = 1$km per hour. Figure 2 shows the initial positions of the vehicles and Figure 3 shows the controlled configuration at time equal to 62.5 hours. After 80 hours, we control vehicles 1 and 3 to be on a smaller 12km by 4.8km box while vehicle 2 stays on the larger box. The separations between vehicles 1 and 2 as well as between vehicles 2 and 3 are still controlled to $c_{s1} = c_{s2} = \pi/2$ as shown in Figure 4. In this case vehicles 1 and 3 travel at lower speed than vehicle 3. After 140 hours, the vehicles are commanded to resume the original pattern on the larger box.

Figure 5 shows the value of the orbit function z_1 of vehicle 1 as a function of time. The value of the orbit function at time t is the length of the semi-major axis of the super-ellipse that the vehicle occupies at time t. Figure 6 shows the separation $\Phi_1 - \Phi_2$ between vehicles 1 and 2 over time. From these figures, one can observe the asymptotic convergence under the control laws. It can be seen that it takes less than 20 hours to set up the pattern on the larger box and about 30 hours to transit from this pattern to the second pattern with vehicles 1 and 3 on the smaller box. The time required for the vehicles to set up the pattern is long mainly because the vehicles are slow and the boxes are large. This is generally the case for underwater gliders which travel at around 1km per hour. At this speed, it takes a vehicle 40 hours to cover the long side of the large box. In our simulation, the initial conditions for the vehicles are arbitrarily given. However, in the field experiments, using other methods such as time optimal control, we set up the initial configurations to be close enough to the desired configuration and use the control laws to maintain the pattern under disturbances.

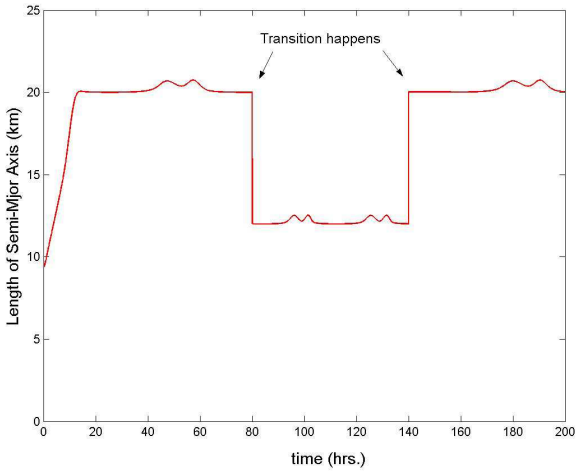

Figure 5. *The orbit value z_1, which is the length of the semi-major axis, as a function of time.*

6 Experiments

In this section we describe how we implement coordinated control schemes on a fleet of real underwater gliders and we present coordinated control results from sea trials with gliders in Buzzards Bay, MA during March 2006.

6.1 *Underwater Gliders*

Underwater gliders are winged submersibles with buoyancy engines (see Rudnick et al. (2004)). The motion of an underwater glider is generated by periodically changing its buoyancy. The lift force from the fixed wings gives the glider maneuvrability. The balance of forces on the glider produces steady gliding motions,

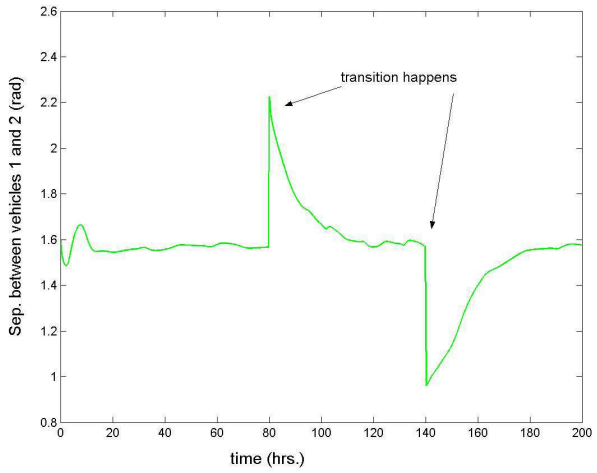

Figure 6. *The curve phase separation between vehicles 1 and 2,* $\Phi_1 - \Phi_2$*, as a function of time.*

either forward and ascending when the glider is positively buoyant or forward and descending when the glider is negatively buoyant. Viewed from the side, because of the switching between up and down motion, the trajectory has a sawtooth shape.

Under the influence of flow, the navigation algorithm on board a glider computes adjustments to direction of motion to compensate for the component of flow that carries the glider off its course towards a waypoint. On Slocum gliders (Rudnick et al. (2004)) used in the Buzzards Bay experiment, heading adjustments are made with a rudder. Effective glider speed towards the waypoint decreases when bearing between flow and the desired course is an obtuse angle. If the perpendicular component of flow is larger than the glider speed, the glider will be carried away by the flow and fail to reach the waypoint.

6.2 *The Glider Coordinated Control System*

In the simulation described in Section 5 we demonstrate the coordinated control algorithm applied to the planar particle model. The real gliders that we use in the field communicate only when they surface (asynchronously) and only with a central on-shore server by means of Iridium satellite. Further, gliders move in three-dimensional space and are challenged by currents of significant magnitude. For development, testing, and implementation on real gliders of control schemes such as the one presented in this paper, we have designed the Glider Coordinated Control System (GCCS), which is described in detail in Paley et al. (2006b).

The GCCS is a cross-platform software suite written in MATLAB that automatically implements feedback control of a glider fleet. It is a modular tool that serves as a simulation testbed as well as a real-time coordinated control system. A particle model like the one described in this paper is used to plan future trajectories and a detailed glider model to estimate glider positions while gliders are underwater. The GCCS trajectory (and waypoint) planner takes as input: parameters that describe the desired coordinated configuration, glider surface position measurements, the glider depth-averaged flow estimates, the glider active waypoint lists, and control parameters. The control algorithm is itself a module so that different control algorithms can be tested. The planner is triggered to initiate a new planning cycle every time a glider surfaces. At the end of a cycle the planner produces an updated waypoint list for each glider; a waypoint here refers to the centre of a circle in the horizontal plane that prescribes the next desired location for the glider. The GCCS remote input/output module implements secure File Transmission Protocol (FTP) for communication to and from the glider data server, e.g., the updated waypoint lists are sent to and the glider surface position measurements are received from the glider data server.

In addition to coordinating the control of gliders in the field, the GCCS has its own glider simulator and can implement the coordinated control on the simulated gliders. It simulates gliders using the detailed glider model with a flow field that can be provided as input (e.g., ocean fields for the region of Monterey

Bay discussed in Section 5). The glider simulator receives its waypoint files from the same data server as real gliders and posts its position measurements (as well as sampled data profiles) to the same data server as real gliders.

The GCCS simulator and planner have been used as a testbed for development and testing of coordinated control schemes under realistic operating conditions. A virtual glider deployment run in March 2006 on ten gliders in Monterey Bay is described in Paley et al. (2006b). The GCCS was used to control six real gliders continuously for 25 days in Monterey Bay in August 2006 as part of the ASAP program.

6.3 *Buzzards Bay Experiment*

We performed coordinated glider sea trials in Buzzards Bay, MA in March 2006 and we present the results of the sea trials here with a focus on coordinated control performance. A detailed description and record of activities during this experiment can be found in Fratantoni and Lund (2006). The experiment served as a good test of the GCCS and provided the opportunity to explore the effect on coordinated control performance of the many constraints and disturbances (e.g., strong tides) to glider operation. Results from previous coordinated control sea trials with underwater gliders are described in Fiorelli et al. (2006). These previous trials, carried out in August 2003 in Monterey Bay, CA, demonstrated control of gliders into triangular formations for sensing and estimating gradients. A precursor to the GCCS was used in August 2003.

The Buzzards Bay experiment ran from March 6 to 17, 2006. Five battery-powered Slocum gliders were deployed during this period. Three of the gliders were put out of service due to hardware problems and environmental hazards. The control law was applied to the remaining two gliders named 'we09' and 'we11'. The goal was to control an invariant pattern on a super-ellipse track within a rectangular region to the west of Naushon Island in Buzzards Bay, see Figure 7(a) and 7(b). The dimensions of the rectangle were approximately 5.9km (along-shore) by 3.3km (cross-shore). Near the Woods Hole Oceanographic Institution (WHOI), this region is the largest area without threats such as underwater rock piles and commercial ship traffic. The super-ellipse track is centred at longitude 70.8003°W, latitude 41.5070°N with its major axis pointing to the along-shore direction at azimuth 40°. The dimension of the super-ellipse is 5.6km by 2.8km. For the invariant pattern, the desired separation between the two gliders is $\pi/3$ measured by curve phase. During the Buzzards Bay experiment, each glider was programmed to spend approximately one hour underwater between surfacing. The average depth of the operation region is about 15 metres. During this one hour period, the glider can accomplish about 20 dives. While the glider is at surface, the communication process takes about 12 minutes to finish. Relative to the flow, the average horizontal speed is about 20 cm/s. Unlike a propeller driven underwater vehicle, this average horizontal speed of the glider is not controlled directly. During the experiment, the control of speed along the original prescribed track was implemented by changing the orbits of the glider. A glider makes slower progress along the original track by moving to an orbit with longer total length and makes faster progress by moving to an orbit with shorter total length. The GCCS generated two waypoints per diving-surfacing cycle for each glider. This means that the gliders were directed along a sequence of two straight line segments every hour.

6.4 *Data and Analysis*

We first plot segments of the trajectories of the two gliders in Figures 7(a) and 7(b). The markers on each segment indicate the GPS locations of the gliders when they surfaced. The underwater position is estimated by the deduced reckoning method. From the position data, we compute the orbit value of the gliders and plot it in Figure 8(a). The curve phase difference between the two gliders is also computed and plotted in Figure 8(b)

To help interpret the results, we plot in Figure 9 the flow speed in the along-shore direction measured (i.e., estimated from measurements) by the two gliders. The measured flow is clearly semi-diurnal. This indicates its tidal nature. The measured flow is also in agreement with predicted tides in Buzzards Bay found in Eldridge (2006) based on historical data. Because the flow strength in the cross-shore direction

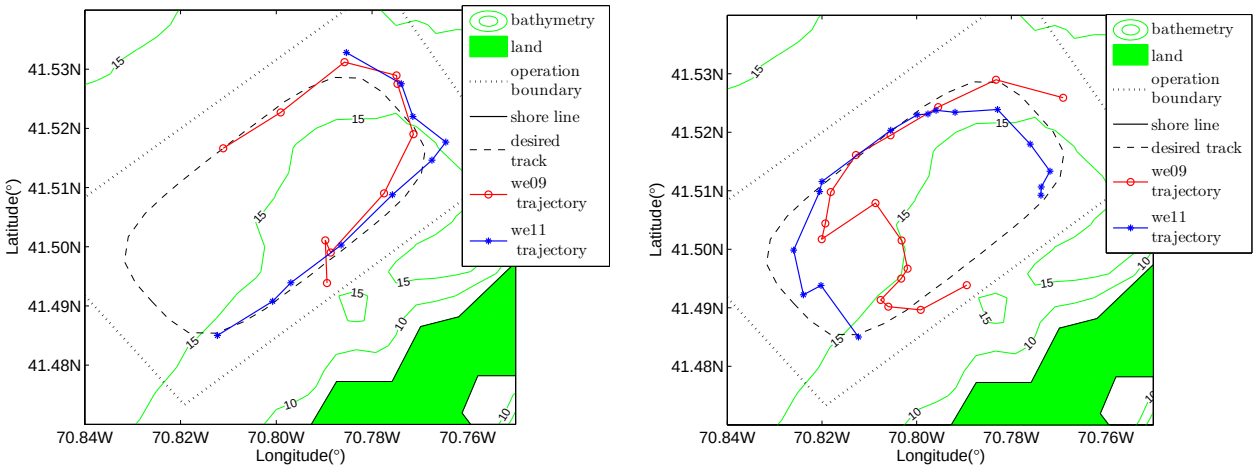

(a) March 13th 19:00 GMT - March 14th 5:35 GMT

(b) March 14th 5:35 GMT - March 14th 22:47 GMT

Figure 7. *Operation region, desired super-ellipse track and glider trajectories between March 13th 19:00 GMT and March 14th 22:47 GMT during the Buzzards Bay experiment in 2006. Both gliders move clockwise. Surfacing positions of we09 are marked by circles and surfacing positions of we11 are marked by stars.*

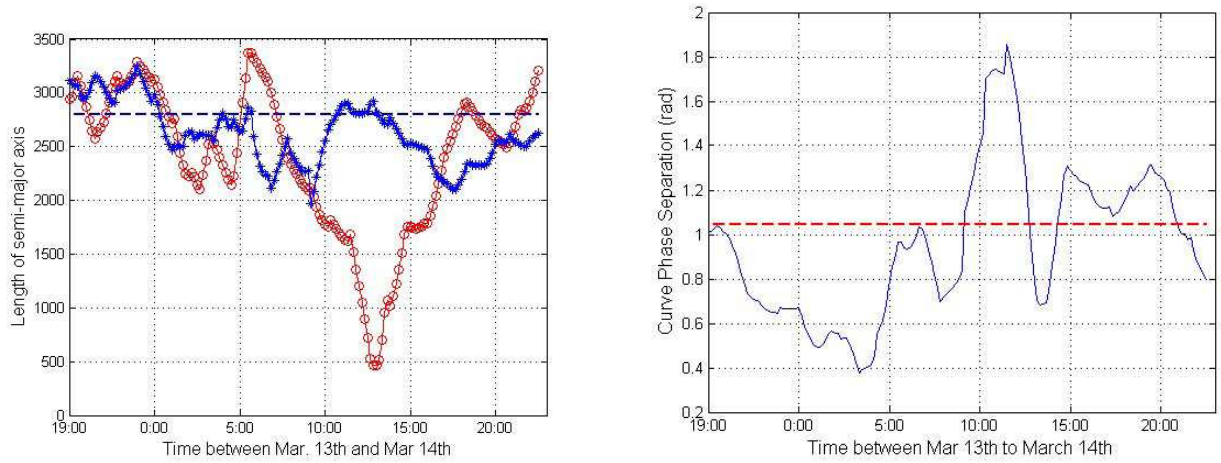

(a) Orbit values of we09 (marked by circles) and we11 (marked by stars).

(b) Curve phase difference between we09 and we11.

Figure 8. *Analysis of the position data. The thick dashed lines indicate the desired value in both cases.*

is significantly weaker, we omit it to simplify our discussion.

We first analyse the twelve hour period from March 13th 19:00 GMT to March 14th 7:00 GMT. From Figure 8(a), we clearly see for both gliders that the orbit value fluctuates around the desired value. The feedback control produced waypoints that kept the gliders near the desired track. From 19:00 GMT to 23:00 GMT on March 13th, the flow was perpendicular to the course for we11 but was aligned with the course of we09 moving northeast. In the inertial frame, the effective speed of we09 was larger than that of we11 which implies that we09 would be catching up to we11. Indeed, we see from Figure 8(b) that the curve phase separation between the two gliders decreased. The flow then reversed its direction and reached its maximum speed between 1:00 GMT and 3:00 GMT on March 14th. From Figure 7(a), we see that during this period, we11 was near the bottom right corner of the super-ellipse, under the influence of strong flow, and we09 took a "shortcut" to the long side of the super-ellipse without traversing the rounded corner. This caused a downward spike in we09's orbit value as shown in Figure 8(a) and further decreased the curve phase difference as shown in Figure 8(b). Then between 3:00 GMT and 7:00 GMT we see that the action of the controller restored the desired curve phase difference. The controller planned a

"wiggling" action for we09 and put we09 on orbit with larger total curve length. This slowed down we09 and restored the desired pattern.

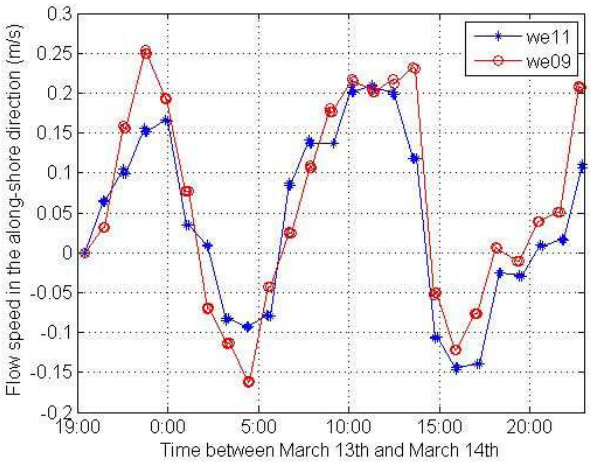

Figure 9. *The flow strength, measured by the gliders, in the along-shore direction from March 13th to March 14th,2006. Positive value indicates flooding current moving northeast. Negative value indicates ebbing current moving southwest.*

During the next period, we see large deviations from the desired invariant pattern between 7:00 GMT and 13:00 GMT on March 14th. From Figure 9 we see that between 7:00 GMT and 13:00 GMT, the flow speed was greater than the averaged glider speed at 20cm/s. This flow was perpendicular to the planned path for glider we09. Following our previous discussions in Section 6.1 about the on-board navigation algorithm, we deduce that we09 was not able to reach the planned waypoints. This is confirmed by Figure 10 where both the planned trajectory and the actual trajectory are plotted for we09 during this period. The glider was carried inward towards the centre of the super-ellipse by strong flooding flow. When the flow attenuated after 13:00 GMT on March 14th, the controller restored the desired pattern. In Figure 8(b), we observe the converging transient of the controlled curve phase between 13:00 GMT and 16:00 GMT on March 14th. An overshoot is produced because the control gain is selected to be high to achieve faster convergence. In Figure 8(a), we can see that the orbit value of both gliders were manipulated by the controller to restore the desired pattern. The overshoot in curve phase difference corresponds to the rapid increase in orbit value of we09 and decrease in orbit value of we11.

We have observed similar patterns in the controlled orbit value and curve phase difference from analysing trajectories during other time periods. The control algorithm and the GCCS performed reliably and repeatably. We can conclude that tidal flow is a most influential factor for the controller performance in this experiment.

6.5 *Discussions and future work*

The "short-cut" action by we11 near a corner of the super-ellipse is related to the fact that each glider travelled along two straight line segments every hour. The length of each line segment is long compared to the radius of curvature at the rounded corner of the super-ellipse used in Buzzards Bay. Therefore, accurate tracking of the curve was not achieved in this experiment. We note that the super-ellipse in Buzzards Bay is much smaller than what was used to study meso-scale ocean features such as in the ASAP experiments discussed in Section 5. For a typical sampling application the dimension of a super-ellipse will be measured in tens of kilometres. In those applications the tracking performance will be much better. Tracking performance can also be improved by reducing the distance between waypoints, hence increasing the number of waypoints for each dive. However, under disturbances such as ocean flow, this might cause the glider to perform unnecessary turns.

In future experiments, it is of interest to further address the challenge of strong currents by incorporating a model for tidal flow in the GCCS. This model should be able to predict the strength and direction of

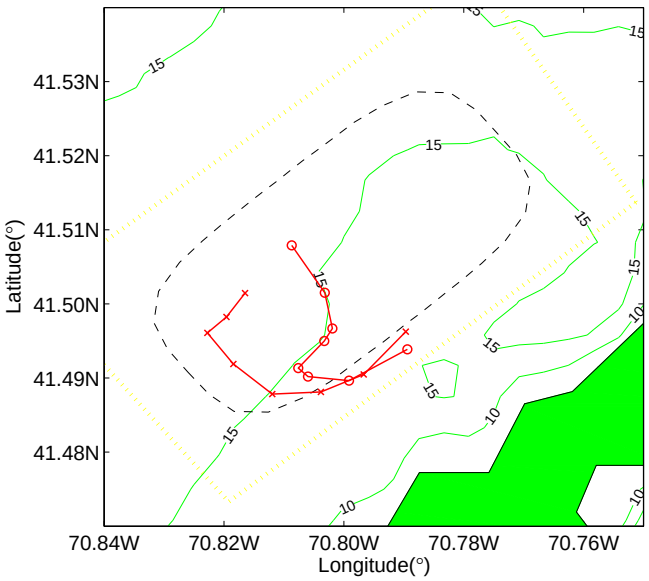

Figure 10. *The planned trajectory of we09 and the actual trajectory between March 14th 5:35 GMT and 13:37 GMT in 2006. The planned trajectory is marked by crosses and the actual trajectory is marked by circles.*

tides so that the gliders can be controlled to avoid moving against strong currents. For applications in which the gliders do not have to strictly stay on the desired track, the motion of the gliders can be planned to only compensate for the non-tidal portion of the flow.

7 Acknowledgement

The authors want to thank R. E. Davis for discussions on controlling underwater gliders for adaptive sampling, I. Shulman and P. Lermusiaux for discussions and sharing ocean model fields and J. Pinner for discussions and help with simulation software. This work was supported in part by ONR grants N00014–02–1–0826, N00014–02–1–0861 and N00014–04–1–0534.

References

S. B. Andersson and J. Park, "Tip steering for fast imaging in AFM", in *Proc. 2005 American Control Conference*, Portland, OR, June 6-10, 2005, pp. 2469–2474.

A. L. Bertozzi, M. Kemp, and D. Marthaler, "Determining environmental boundaries: Asynchronous communication and physical scales", in *Cooperative Control, A Post-Workshop Volume: 2003 Block Island Workshop on Cooperative Control*, V. Kumar, N. Leonard, and A. Morse, Eds. Springer, 2005, pp. 35–42.

J. Clark and R. Fierro, "Cooperative hybrid control of robotic sensors for perimeter detection and tracking", in *Proc. 2006 American Control Conference*, Portland, OR, June 6-10, 2005, pp. 3500–3505.

G. Eldridge, *Eldridge Tide and Pilot Book, 132nd Ed.* Robert Eldridge White Jr and Linda Foster White, Boston, MA 2006.

E. Fiorelli, N. E. Leonard, P. Bhatta, D. A. Paley, R. Bachmayer, and D. M. Fratantoni, "Multi-AUV control and adaptive sampling in Monterey Bay", *IEEE Journal of Oceanic Engineering*, vol. 31, no. 3, 2006.

D. M. Fratantoni and J. M. Lund, "Glider operations in Buzzard's Bay, MA", *Technical report of the Autonomous Systems Lab, Woods Hole Oceanographic Institution*, [Online] `http://asl.whoi.edu`, March, 2006.

M. A. Hsieh and V. Kumar, "Pattern generation with multiple robots", in *Proc. 2006 IEEE International Conference on Robotics and Automation*, Orlando, FL, 2006, pp. 2442–2447,.

E. W. Justh and P. S. Krishnaprasad, "A simple control law for UAV formation flying", *ISR Technical Report TR2002-38*, 2002.

E. W. Justh and P. S. Krishnaprasad, "Equilibria and steering laws for planar formations", *System and Control Letters*, vol. 52, no. 1, pp. 25–38, 2004.

H. Khalil, *Nonlinear Systems, 3rd Ed.* Prentice Hall, 2001.

N. E. Leonard, D. Paley, F. Lekien, R. Sepulchre, D. M. Fratantoni, and R. Davis, "Collective motion, sensor networks and ocean sampling", *Proceedings of IEEE:* Special Issue on the Emerging Technology of Networked Control Systems, in print 2007.

MBARI, Autonomous Ocean Sampling Network, [Online] `http://www.mbari.org/aosn/MontereyBay2003/`

A. Micaelli and C. Samson, "Trajectory tracking for unicycle-type and two-steering-wheels mobile robots", *INRIA report 2097*, 1993.

D. A. Paley, N. E. Leonard, and R. Sepulchre, "Collective motion of self-propelled particles: Stabilising symmetric formations on closed curves", in *Proc. 45th IEEE Conference on Decision and Control*, San Diego, CA, 2006, pp. 5067–5072.

D. A. Paley, F. Zhang and N. E. Leonard, "Glider control for ocean sampling: The glider coordinated control system", submitted to *IEEE Transaction on Control System Technology*.

Princeton University, Adaptive Sampling and Prediction, [Online]`http://www.princeton.edu/~dcsl/asap/`

D. L. Rudnick, R. E. Davis, C. C. Eriksen, D. M. Fratantoni, and M. J. Perry, "Underwater gliders for ocean research", *Marine Technology Society Journal*, vol. 38, pp. 48–59, 2004.

S. Susca, S. Martinez, and F. Bullo, "Monitoring environmental boundaries with a robotic sensor network", in *Proc. 2006 American Control Conference*, Minneapolis, MN, 2006, pp. 2072–2077.

D. Zarzhitsky, D. F. Spears, and W. M. Spears, "Swarms for chemical plume tracing", in *Proc. of 2005 IEEE Symposium on Swarm Intelligence*, Pasadena, CA, 2005, pp. 249–256.

F. Zhang, E. W. Justh, and P. S. Krishnaprasad, "Boundary following using gyroscopic control", in *Proc. of 43rd IEEE Conference on Decision and Control*, Atlantis, Paradise Island, Bahamas, 2004, pp. 5204–5209.

F. Zhang and P. S. Krishnaprasad, "Co-ordinated orbit transfer of satellite clusters", in *Annals of the New York Academy of Sciences*, vol. 1017, pp. 112–137, 2004.

F. Zhang and N. E. Leonard, "Generating contour plots using multiple sensor platforms", in *Proc. of 2005 IEEE Symposium on Swarm Intelligence*, Pasadena, CA, 2005, pp. 309–314.

F. Zhang and N. E. Leonard, "Coordinated patterns on smooth curves", in *Proc. of 2006 IEEE International Conference on Networking, Sensing and Control*, Ft. Lauderdale, FL, 2006, pp. 434–440.

Appendix A: The development of control law

We want to compute the time derivative of the Lyapunov function in (26) along the controlled system trajectory. To simplify the process, the time derivatives of each term in equation (26) is computed separately. We use f_{zi} and f_{sj} as abbreviated notations for $f_{zi}(z_i)$ and $f_{sj}(\Phi_j - \Phi_{j+1})$.

First, similar to Zhang et al. (2004) and Zhang and Leonard (2005), we have

$$\begin{aligned}
&\frac{\mathrm{d}}{\mathrm{d}t}\left(-\log\left(\cos^2\frac{\phi_i}{2}\right)+h_{zi}(z_i)\right)\\
&=\frac{\alpha_i\sin\frac{\phi_i}{2}}{\cos\frac{\phi_i}{2}}\left(\kappa_{1i}\cos\phi_i+\kappa_{2i}\sin\phi_i-u_i-2f_{zi}\parallel\nabla z_i\parallel\cos^2\frac{\phi_i}{2}\right)\\
&=-\mu_1\frac{\alpha_i\sin^2\frac{\phi_i}{2}}{\cos\frac{\phi_i}{2}}+\frac{\alpha_i\sin\frac{\phi_i}{2}}{\cos\frac{\phi_i}{2}}\bar{u}_i\ ,
\end{aligned}\tag{A1}$$

where we let, for $i = 1, 2, ..., N$,

$$\bar{u}_i = \mu_1 \sin\frac{\phi_i}{2} + \kappa_{1i}\cos\phi_i + \kappa_{2i}\sin\phi_i - 2f_{zi}\parallel\nabla z_i\parallel\cos^2\frac{\phi_i}{2} - u_i \tag{A2}$$

and $\mu_1 > 0$ is a constant. Next, for $j = 1, 2, ..., N-1$,

$$\frac{\mathrm{d}}{\mathrm{d}t}h_{sj}(\Phi_j - \Phi_{j+1}) = (\dot{\Phi}_j - \dot{\Phi}_{j+1})f_{sj} \tag{A3}$$

where

$$\begin{aligned}
&\dot{\Phi}_j - \dot{\Phi}_{j+1} \\
&= 2\pi\left(\frac{\alpha_j}{L_j}\cos\phi_j - \frac{\alpha_{j+1}}{L_{j+1}}\cos\phi_{j+1} - \right. \\
&\left.\frac{\alpha_j P_j}{L_j}\parallel\nabla z_j\parallel\sin\phi_j + \frac{\alpha_{j+1}P_{j+1}}{L_{j+1}}\parallel\nabla z_{j+1}\parallel\sin\phi_{j+1}\right) \\
&= 2\pi\left(\frac{\alpha_j}{L_j} - \frac{\alpha_{j+1}}{L_{j+1}} - \frac{\alpha_j}{L_j}2\sin^2\frac{\phi_j}{2} + \frac{\alpha_{j+1}}{L_{j+1}}2\sin^2\frac{\phi_{j+1}}{2} - \right. \\
&\left.\frac{\alpha_j P_j}{L_j}\parallel\nabla z_j\parallel\sin\phi_j + \frac{\alpha_{j+1}P_{j+1}}{L_{j+1}}\parallel\nabla z_{j+1}\parallel\sin\phi_{j+1}\right).
\end{aligned} \tag{A4}$$

We also have, for $j = 1, 2, ..., N-1$,

$$\begin{aligned}
&\frac{\mathrm{d}}{\mathrm{d}t}\left(\frac{1}{2}\left(\frac{\alpha_j}{L_j} - \frac{\alpha_{j+1}}{L_{j+1}}\right)^2\right) \\
&= \left(\frac{\alpha_j}{L_j} - \frac{\alpha_{j+1}}{L_{j+1}}\right)\left(\frac{v_j}{L_j} - \frac{v_{j+1}}{L_{j+1}} + \frac{\alpha_j^2}{L_j^2}\frac{\partial L_j}{\partial z_j}\parallel\nabla z_j\parallel\sin\phi_j - \right. \\
&\left.\frac{\alpha_{j+1}^2}{L_{j+1}^2}\frac{\partial L_{j+1}}{\partial z_{j+1}}\parallel\nabla z_{j+1}\parallel\sin\phi_{j+1}\right).
\end{aligned} \tag{A5}$$

We let, for $i = 1, 2, ..., N$,

$$\bar{v}_i = v_i + \frac{\alpha_i^2}{L_i}\frac{\partial L_i}{\partial z_i}\parallel\nabla z_i\parallel\sin\phi_i\,. \tag{A6}$$

Then, for $j = 1, 2, ..., N-1$,

$$\begin{aligned}
&\frac{\mathrm{d}}{\mathrm{d}t}\left(h_{sj}(\Phi_j - \Phi_{j+1}) + \left(\frac{\alpha_j}{L_j} - \frac{\alpha_{j+1}}{L_{j+1}}\right)^2\right) \\
&= (\dot{\Phi}_j - \dot{\Phi}_{j+1})f_{sj} + \left(\frac{\alpha_j}{L_j} - \frac{\alpha_{j+1}}{L_{j+1}}\right)\left(\frac{\bar{v}_j}{L_j} - \frac{\bar{v}_{j+1}}{L_{j+1}}\right).
\end{aligned} \tag{A7}$$

If we add equations (A1) and (A7) and sum over i and j, the following term appears and can be simplified as follows:

$$\sum_{i=1}^{N}\frac{\alpha_i\sin\frac{\phi_i}{2}}{\cos\frac{\phi_i}{2}}\bar{u}_i + \sum_{j=1}^{N-1}\left(-\frac{\alpha_j}{L_j}2\sin^2\frac{\phi_j}{2} + \frac{\alpha_{j+1}}{L_{j+1}}2\sin^2\frac{\phi_{j+1}}{2} - \right.$$

$$\frac{\alpha_j P_j}{L_j} \parallel \nabla z_j \parallel \sin\phi_j + \frac{\alpha_{j+1} P_{j+1}}{L_{j+1}} \parallel \nabla z_{j+1} \parallel \sin\phi_{j+1} \Bigg) 2\pi f_{sj}$$
$$= \sum_{i=1}^{N} \frac{\alpha_i \sin\frac{\phi_i}{2}}{\cos\frac{\phi_i}{2}} \left(\bar{u}_i - 2\pi (f_{si} - f_{s(i-1)}) \left(\frac{1}{L_i} \sin\phi_i + 2\frac{P_i}{L_i} \parallel \nabla z_i \parallel \cos^2\frac{\phi_i}{2} \right) \right) \tag{A8}$$

where $f_{s0} = f_{sN} = 0$. We let, for $i = 1, 2, ..., N$,

$$\bar{u}_i = 2\pi (f_{si} - f_{s(i-1)}) \left(\frac{1}{L_i} \sin\phi_i + 2\frac{P_i}{L_i} \parallel \nabla z_i \parallel \cos^2\frac{\phi_i}{2} \right) \tag{A9}$$

so that equation (A8) vanishes. Then

$$\dot{V} = \sum_{i=1}^{N} \left(-\mu_1 \frac{\alpha_i \sin^2\frac{\phi_i}{2}}{\cos\frac{\phi_i}{2}} \right) + f_a(\alpha_1) v_1 +$$
$$\sum_{j=1}^{N-1} \left(\frac{\alpha_j}{L_j} - \frac{\alpha_{j+1}}{L_{j+1}} \right) \left(\frac{\bar{v}_j}{L_j} - \frac{\bar{v}_{j+1}}{L_{j+1}} + 2\pi f_{sj} \right). \tag{A10}$$

We let, for $j = 1, 2, ..., N-1$,

$$\frac{\bar{v}_j}{L_j} - \frac{\bar{v}_{j+1}}{L_{j+1}} + 2\pi f_{sj} = -\mu_2 \left(\frac{\alpha_j}{L_j} - \frac{\alpha_{j+1}}{L_{j+1}} \right) \tag{A11}$$

and

$$v_1 = -\mu_3 f_a(\alpha_1) \tag{A12}$$

where $\mu_2 > 0$ and $\mu_3 > 0$. Then

$$\dot{V} = \sum_{i=1}^{N} \left(-\mu_1 \frac{\alpha_i \sin^2\frac{\phi_i}{2}}{\cos\frac{\phi_i}{2}} \right) - \sum_{j=1}^{N-1} \mu_2 \left(\frac{\alpha_j}{L_j} - \frac{\alpha_{j+1}}{L_{j+1}} \right)^2$$
$$-\mu_3 f_a(\alpha_1)^2 \leq 0 \, . \tag{A13}$$

From (A9) and (A2), we can derive the steering control law as

$$u_i = \kappa_{1i} \cos\phi_i + \kappa_{2i} \sin\phi_i - 2 f_{zi} \parallel \nabla z_i \parallel \cos^2\frac{\phi_i}{2} -$$
$$2\pi (f_{si} - f_{s(i-1)}) \left(\frac{1}{L_i} \sin\phi_i + 2\frac{P_i}{L_i} \parallel \nabla z_i \parallel \cos^2\frac{\phi_i}{2} \right)$$
$$+\mu_1 \sin\frac{\phi_i}{2} \tag{A14}$$

for $i = 1, 2, ..., N$. The speed control for the first particle is given by (A12). Apply (A6) for $i = 1$, we have

$$\bar{v}_1 = v_1 + \frac{\alpha_1^2}{L_1} \frac{\partial L_1}{\partial z_1} \parallel \nabla z_1 \parallel \sin\phi_1. \tag{A15}$$

Equation (A11) allows us to compute $\bar{v}_{j+1}$ from $\bar{v}_j$, i.e.,

$$\bar{v}_{j+1} = \frac{L_{j+1}}{L_j} \bar{v}_j + 2\pi f_{sj} L_{j+1} + \mu_2 \left(\frac{L_{j+1}}{L_j} \alpha_j - \alpha_{j+1} \right). \tag{A16}$$

Then the speed control v_{j+1} is found by applying (A6) for $i = j + 1$, and we have

$$v_{j+1} = \bar{v}_{j+1} - \frac{\alpha_{j+1}^2}{L_{j+1}} \frac{\partial L_{j+1}}{\partial z_{j+1}} \| \nabla z_{j+1} \| \sin \phi_{j+1}. \tag{A17}$$